SEMINAR REPORT

on

TRANSPARENT ELECTRONICS

Submitted by

SHYAM DAVID C V

In partial fulfillment of the requirements for the award of the degree of Bachelor of Technology in

ELECTRONICS AND COMMUNICATION ENGINEERING

of

COCHIN UNIVERSITY OF SCIENCE AND TECHNOLOGY

SEPTEMBER 2010

DEPARTMENT OF ELECTRONICS AND COMMUNICATION ENGINEERING

Toc H INSTITUTE OF SCIENCE & TECHNOLOGY

Arakkunnam P.O, Ernakulam District, KERALA –682 313

Toc H INSTITUTE OF SCIENCE & TECHNOLOGY

Arakkunnam P.O, Ernakulam District, Kerala – 682 313.

DEPARTMENT OF ELECTRONICS & COMMUNICATION ENGINEERING

CERTIFICATE

This is to certify that the seminar entitled *"TRANSPARENT ELECTRONICS"* submitted by *"SHYAM DAVID C V"* of semester VII is a bonafide account of the work done by him under our supervision during the academic year 2010 - 2011.

Seminar Guide   **Head of the Department**

Head of the Institution

ACKNOWLEDGEMENT

The satisfaction and euphoria that successful completion of any task would be incomplete sans the mention of the people who made it possible, whose constant guidance and encouragement crown our effort with success.

First, I would like to express my whole hearted thanks to the invisible, the indomitable **God** for His blessings showered upon me in enabling me to complete this seminar synopsis on time.

I would like to extend my heartiest thanks to the **Management** of our college, who provided me with the necessities for the completion of the seminar synopsis. I feel highly privileged in making a mention of **Dr. V. Job Kuruvilla (Principal, TIST)** for his cooperation and help. I am also deeply privileged in taking this opportunity to make a mention of **Prof. (Col.) P.M. Xavier (Vice Principal, TIST)** for his cooperation and guidance.

I would also like to extend my heartfelt thanks to **Asst. Prof. Deepa Elizabeth George (HOD, ECE)** for the inspiration inculcated in me and for the apt guidance.

It would be a grave error if I do not make a mention of my seminar guides **Ms. Smita Damodaran** & **Ms. Sreelakshmi V**. Before culminate, I would like to extend my heartfelt gratitude to all the teachers and staff of the Department of Electronics & Communication, TIST for their cooperation and support.

Last but not the least, I thank all others, and especially my family members and my classmates who in one way or another helped me in the successful completion of this work.

ABSTRACT

Transparent electronics is an emerging science and technology field focused on producing 'invisible' electronic circuitry and opto-electronic devices. Applications include consumer electronics, new energy sources, and transportation; for example, automobile windshields could transmit visual information to the driver. Glass in almost any setting could also double as an electronic device, possibly improving security systems or offering transparent displays. In a similar vein, windows could be used to produce electrical power. Other civilian and military applications in this research field include real-time wearable displays. As for conventional Si/III–V-based electronics, the basic device structure is based on semiconductor junctions and transistors. However, the device building block materials, the semiconductor, the electric contacts, and the dielectric/passivation layers, must now be transparent in the visible –a true challenge! Therefore, the first scientific goal of this technology must be to discover, understand, and implement transparent high-performance electronic materials. The second goal is their implementation and evaluation in transistor and circuit structures. The third goal relates to achieving application-specific properties since transistor performance and materials property requirements vary, depending on the final product device specifications. Consequently, to enable this revolutionary technology requires bringing together expertise from various pure and applied sciences, including materials science, chemistry, physics, electrical/electronic/circuit engineering, and display science.

INDEX

LIST OF FIGURES

Sl.No.   Title   Page No.

1. INTRODUCTION

Transparent electronics is an emerging science and technology field focused on producing 'invisible' electronic circuitry and opto-electronic devices. Applications include consumer electronics, new energy sources, and transportation; for example, automobile windshields could transmit visual information to the driver. Glass in almost any setting could also double as an electronic device, possibly improving security systems or offering transparent displays. In a similar vein, windows could be used to produce electrical power. Other civilian and military applications in this research field include real-time wearable displays. As for conventional Si/III–V-based electronics, the basic device structure is based on semiconductor junctions and transistors. However, the device building block materials, the semiconductor, the electric contacts, and the dielectric/passivation layers, must now be transparent in the visible –a true challenge! Therefore, the first scientific goal of this technology must be to discover, understand, and implement transparent high-performance electronic materials. The second goal is their implementation and evaluation in transistor and circuit structures. The third goal relates to achieving application-specific properties since transistor performance and materials property requirements vary, depending on the final product device specifications. Consequently, to enable this revolutionary technology requires bringing together expertise from various pure and applied sciences, including materials science, chemistry, physics, electrical /electronic/ circuit engineering, and display science.

During the past 10 years, the classes of materials available for transparent electronics applications have grown dramatically. Historically, this area was dominated by transparent conducting oxides (oxide materials that are both electrically conductive and optically transparent) because of their wide use in antistatic coatings, touch display panels, solar cells, flat panel displays, heaters,

defrosters, 'smart windows' and optical coatings. All these applications use transparent conductive oxides as passive electrical or optical coatings. The field of transparent conducting oxide (TCO) materials has been reviewed and many treatises on the topic are available. However, more recently there have been tremendous efforts to develop new active materials for functional transparent electronics. These new technologies will require new materials sets, in addition to the TCO component, including conducting, dielectric and semiconducting materials, as well as passive components for full device fabrication.

2. COMBINING OPTICAL TRANSPARENCY WITH ELECTRICAL CONDUCTIVITY

Transparent conductors are neither 100% optically transparent nor metallically conductive. From the band structure point of view, the combination of the two properties in the same material is contradictory: a transparent material is an insulator which possesses completely filled valence and empty conduction bands; whereas metallic conductivity appears when the Fermi level lies within a band with a large density of states to provide high carrier concentration.

Efficient transparent conductors find their niche in a compromise between a sufficient transmission within the visible spectral range and a moderate but useful in practice electrical conductivity. This combination is achieved in several commonly used oxides – In_2O_3, SnO_2, ZnO and CdO. In the undoped stoichiometric state, these materials are insulators with optical band gap of about 3 eV. To become a transparent conducting oxide (TCO), these TCO hosts must be degenerately doped to displace the Fermi level up into the conduction band.

The key attribute of any conventional n-type TCO host is a highly dispersed single freeelectron- like conduction band (Figure 1). Degenerate doping then provides both (i) the high mobility of extra carriers (electrons) due to their small effective mass and (ii) lowoptical absorption due to the lowdensity of states in the conduction band. The high energy dispersion of the conduction band also ensures a pronounced Fermi energydisplacement up above the conduction band minimum, the Burstein–Moss (BM) shift. The shift helps to broaden the optical transparency window and to keep the intense optical transitions from the valence band out of the visible range. This is critical in oxides which are not transparent throughout the entire visible spectrum, for example, in CdO where the optical (direct) band gap is 2.3 eV.
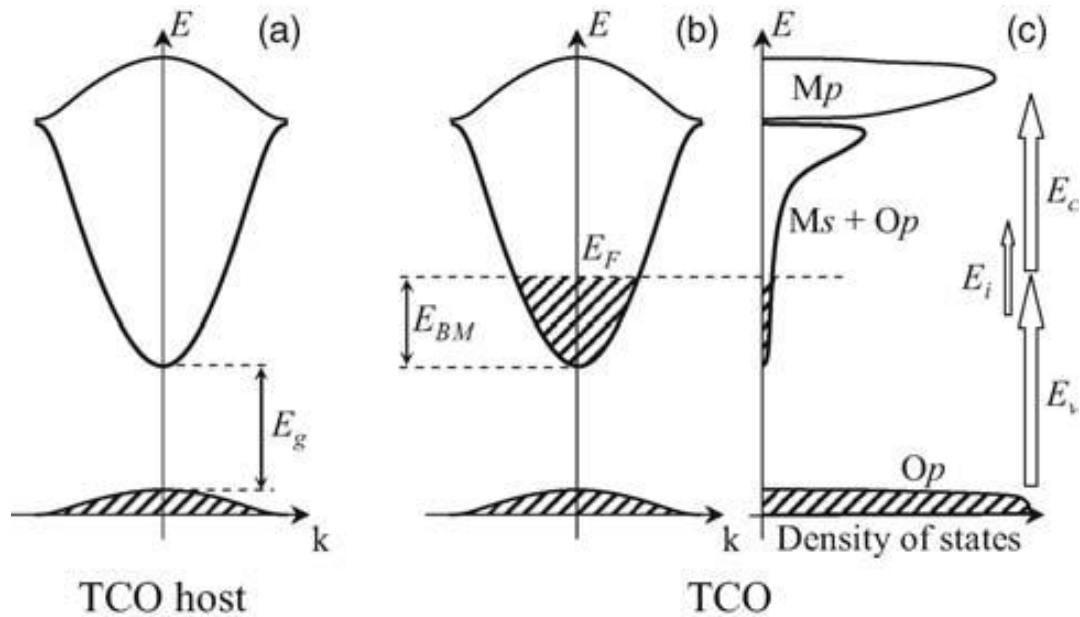
Fig.1: (a) Schematic electronic band structure of aTCOhost – an insulator with a band gap Eg and a dispersed parabolic conduction band which originates from interactions between metal s and oxygen p states. (b) and (c) Schematic band structure and density of states of a TCO, where a degenerate doping displaces the Fermi level (EF) via a Burstein-Moss shift, EBM, making the system conducting. The shift gives rise to inter-band optical transitions from the valence band, Ev, and from the partially filled conduction band up into the next empty band, Ec, as well as to intraband transitions within the conduction band, Ei

Achieving the optimal performance in a TCO is a challenging because of the complex interplay between the electronic and optical properties. The large carrier concentrations desired for a good conductivity may result in an increase of the optical absorption (i) at short wavelengths, due to inter-band transitions from the partially filled conduction band and (ii) at long wavelengths, due to intra-band transitions within this band. In addition, plasma oscillations may affect the optical properties by reflecting the electromagnetic waves of frequency below that of the plasmon. Furthermore, ionized impurity scattering on the electron donors (native

point defects or substitutional dopants) have a detrimental effect on the charge transport, while the structural relaxation around the impurities may alter the electronic and optical properties of the host, leading to a nonrigid-band shift of the Fermi level. We demonstrate here that a thorough understanding of the microscopic properties of metal oxides provides an insight into the underlying phenomena and also suggests that the range of efficient TCO materials can be significantly broadened.

3.Electronic Properties of Conventional TCO Hosts

Conventional n-type TCO hosts (In2O3, SnO2, CdO and ZnO) share similar chemical, structural and electronic properties. Exclusively oxides of the post-transition metals with $(n-1)d^{10}ns^2$ electronic configurations, they have densely packed structures with four- or six-coordinate metal ions. Strong interactions between the oxygen 2p and metal ns orbitals give rise to electronic band structures qualitatively similar for all these oxides (Figures 1 and 2): the bonding and nonbonding O 2p states form the valence band while the conduction band arises from the antibonding Ms–Op interactions. The empty p states of the metal ion form the following band at a higher energy. The partial density of states plots
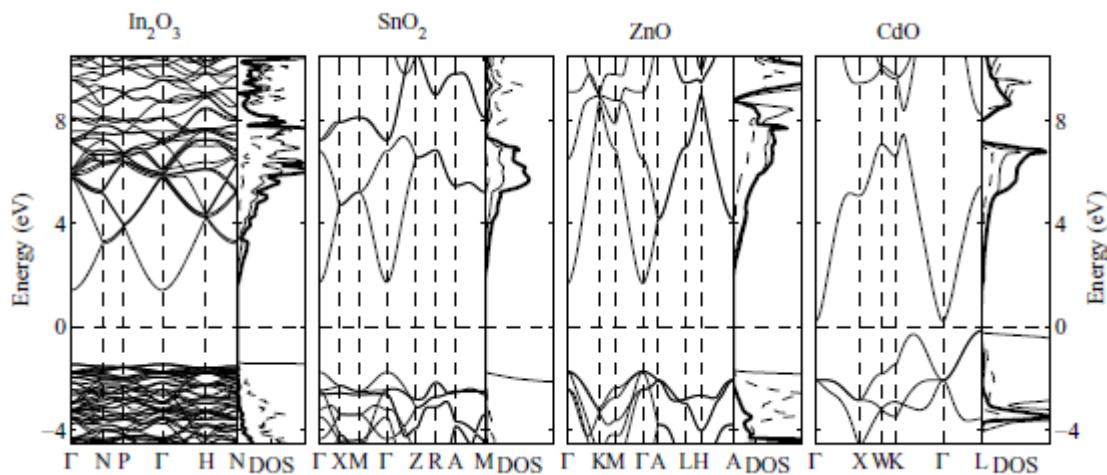
Fig.2: Electronic band structure and partial density of states of TCO hosts, In2O3, SnO2, ZnO and CdO, as obtained within the screened-exchange local-density approximation. In the density of states plots, the thick, dashed and thin lines represent metal s, metal p and oxygen p states, respectively. The plots should be compared with the schematic band structure shown in Figure 1(a)

(Figure 2), reveal that the oxygen 2p and metal ns states make similar contributions to the conduction band. This provides a three-dimensional Ms–Op network for charge transport once extra carriers fill the band.

Ms–Op interactions result in a gap between the valence and the conduction bands. In ZnO, the gap is direct whereas in CdO, In2O3 or SnO2 the valence band maximum is at the L point ([111]), H point ([1 11]) or R point ([011]), respectively, giving rise to an indirect band gap of 0.4 eV, 2.6 eVor 2.7 eV, respectively. Table 1 lists the direct opticalband gaps which are of primary importance for TCO applications. These values are obtained from the electronic band structure calculations within screened-exchange local density approximation (sX-LDA) , which gives good agreement with the reported experimental values (3.5–3.7 eV for In2O3, 2.3 eV for CdO, 3.1–3.6 eV for ZnO and 3.6–4.0 eV for SnO2).

Table 1: Basic properties of conventional TCO hosts. The optical band gaps and the electron effective masses are determined within screened-exchange local-density approximation (sX-LDA) [19]. Anisotropy of the electron effective mass is defined as $\delta = \left(m^{[1\bar{0}0]} + m^{[010]} \right)/2m^{[001]}$.

| Oxide	Lattice	Coordination of		Optical (direct) band gap (eV)	Electron effective mass, m_e			Effective mass anisotropy
		cation	anion		$m^{[100]}$	$m^{[010]}$	$m^{[001]}$	
ZnO	Wurtzite	4	4	3.41	0.35	0.35	0.35	1.008
CdO	Rocksalt	6	6	2.28	0.23	0.23	0.23	1.000
In$_2$O$_3$	Byxbyite	6	4	3.38	0.28	0.28	0.28	1.000
SnO$_2$	Rutile	6	3	3.50	0.33	0.33	0.28	1.179

TheMs–Op overlap also determines the energy dispersion of the conduction band in these materials.Within the framework of k p theory [30], the electron effective mass can be found within the second-order perturbation:

$$\frac{m_e}{m_{ii}^{(c)}} = 1 + \frac{2}{m_e} \sum_{l \neq c} \frac{|\langle u^{(c)}|\hat{p}_i|u^{(l)}\rangle|^2}{E^{(c)} - E^{(l)}}, \qquad (1.1)$$

where p is the momentum operator, $|u^{(l)}\rangle$ is the Bloch wave function of the l's band at the G point (wave vector k=0) and $E^{(l)}$ is its energy. Band label c represents the conduction band, while the sum runs over all other bands. In the oxides under consideration here, the electron effective mass is less than the mass of the electron, me. As it follows from Equation (1.1), it is determined primarily by the valence band contributions $(E^{(l)} < E^{(c)})$, i.e. by the oxygen 2p states.

From the orbital symmetry considerations (Figure 3) coordination of cations by the oxygen atoms have little effect on the Ms–Op overlap owing to the spherical symmetry of the s orbitals. The largest Ms–Op overlap is attained when the oxygen atom is coordinated octahedrally by the cations, i.e. when each of the
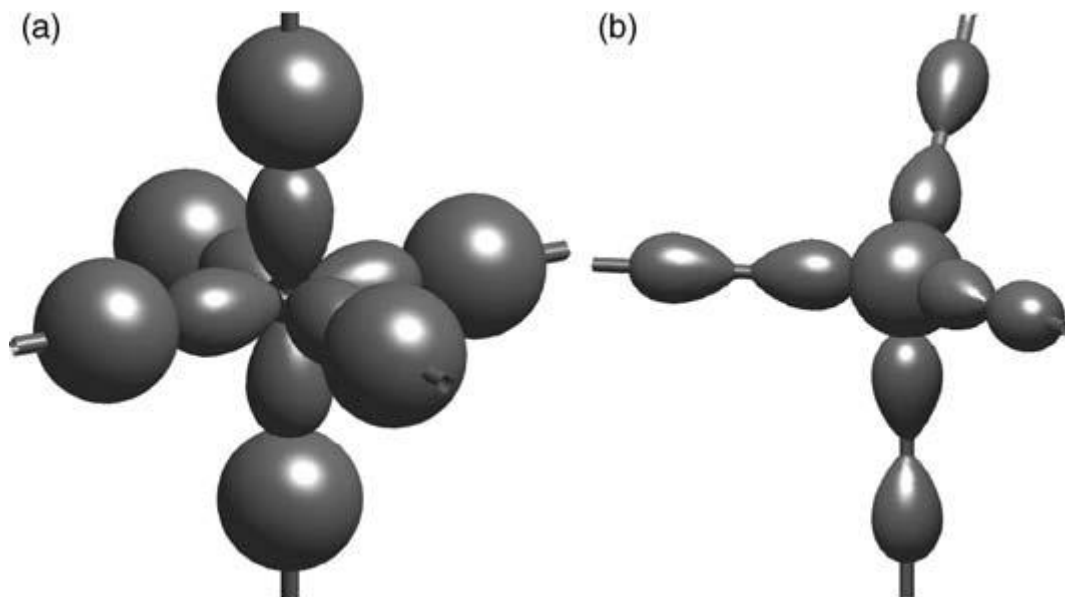
Fig.3: Octahedral coordination of oxygen atoms by cations (a) provides the largest overlap between the oxygen px, py and pz orbitals and the s orbitals of the metal ions. Coordination ofcations by oxygen atoms as well as local distortions (b) have little effect on the Ms–Op overlap owing to the spherical symmetry of the metal s orbitals

oxygen px, py and pz orbitals connects two s orbitals (Figure 3). Accordingly, the octahedral coordination of the oxygen atoms in rocksalt CdO gives rise to the largest dispersion and, hence, the smallest electron effective mass among the TCO materials (Table 1). However, it was found that variations in the oxygen coordination and strong distortions in the polyhedra have little effect on the electron effective mass which varies insignificantly when the symmetry of the same-cation oxide is changed. For example, for ZnO in rocksalt (octahedral coordination) or wurtzite (tetrahedral coordination) structures, and for In_2O_3 in $Ia\bar{3}$ (byxbyite), $R\bar{3}c$ (corundum) or $I2_13$ structures, the effective masses vary by about 15%. Moreover, the effective mass remains nearly isotropic in all phases of the oxides – including those with irregular atomic arrangements or large structural voids.

Little sensitivity of the Ms–Op overlap and, hence, of the electron effective mass to structural variations may explain the success of amorphous TCOs whose optical and electrical properties remain similar to those in the crystalline state. This is in marked contrast to, for example, amorphous Si where the directional interactions between the conduction p orbitals lead to strong anisotropy of the transport properties which are sensitive to the orbital overlap and, hence, to the distortions in the atomic chains.

Thus, the network of alternating metal and oxygen atoms ensures the small electron effective mass in the TCO hosts. A direct overlap between metal s orbitals is not possible in these materials except for SnO_2 where Sn atoms may bond along the edge sharing rutile chain (along the [001] crystallographic direction). However, the fact that the calculated (Table 1) and the observed [38] electron effective mass in this oxide is nearly isotropic suggests that the s–s interactions do not govern the transport properties of TCOs.

In the next section, where we will consider the conversion of the TCO hosts from insulators to conductors, the Ms–Op origin of the conduction band will play a critical role.

4. Carrier Generation in Conventional TCO Hosts

The optical and transport properties of a conventional TCO are governed by the efficiency and the specifics of the carrier generation mechanism employed. Even in the most favorable situation, i.e. when the effects of dopant solubility, clustering, secondary phase formation and charge compensation can be avoided, large concentrations of electron donors (substitutional dopants and/or native point defects) not only promote the charge scattering but also may significantly alter the electronic band structure of the host oxide, leading to a nonrigid band shift of the Fermi level. A detailed band structure analysis of the doped oxides helps to elucidate the role of different factors involved.

4.1 SUBSTITUTIONAL DOPING

Substitutional doping with aliovalent ions is the most widely used approach to generate free carriers in TCO hosts. Compared with native point defects, it allows a better control over the resulting optical and transport properties as well as better environmental stability of the TCO films. Traditionally, same-period, next-row elements, e.g, Sn^{4+} for In^{3+} and In^{3+} for Cd^{2+}, are thought to provide better compatibility and, thus, less disturbance in the host crystal and electronic structure.However, other dopants may prove beneficial for optimizing the properties for a specific application. For example, transparent conducting ZnO films have been prepared by doping with Group III (Al, Ga, In and B), Group IV (Si, Ge, Ti, Zr and Hf) and a Group VII element (F substituted at an oxygen site), giving rise to a wide range of electrical conductivities.

Here we will give a detailed consideration to rocksalt CdO, where the high crystal symmetry and the densely packed structure ensures the most uniform charge density distribution via the isotropicMs–Op network. Compared with more

complex In_2O_3 or SnO_2, one can expect fewer ionized and neutral scattering centers and, hence, longer relaxation times. At the same time, introduction of dopants into the densely packed structure may significantly influence the Cds–2p hybridization and, therefore, alter the structural, electronic and optical properties of the host. A systematic comparison of CdO doped with In, Ga, Sc or Y, whose ionic radius and electronic configuration differ from those of the host cation, has revealed that:

(i) Substitutional dopants with smaller ionic radii compared with that of Cd shrink the lattice. The shrinkage, however, is not as large as expected from the Vegard's law weighted average of the six-coordinated X_{3+} and Cd_{2+} ionic radii. Moreover, in the case of X=In or Y, the lattice parameter is similar or even slightly greater than that of CdO (Table 2). One of the possible explanations is that the doping-induced shrinkage is compensated by an expansion mechanism which originates from the antibonding character of the conduction band formed from Cd 5s and O 2p states. The antibonding mechanism is dominant in In or Y doped CdO, while Sc or Ga have sufficiently smaller ionic radii to weaken Ms–Op hybridization and, thus, to compress the lattice.

(ii) Weaker Cd5s–O2p hybridization associated with strong structural relaxation around dopant with a smaller ionic radius results in a smaller optical band gap (Table 2). Doping with Ga whose ionic radius is significantly smaller than that of Cd, reduces the optical band gap (to 2.53 eV) so that it becomes smaller than the one in undoped CdO (2.82 eV) – despite the doping-introduced BM shift of 2.3 eV. The smallest optical band gap in Ga-doped CdO as compared with In, Y and Sc cases was observed experimentally.
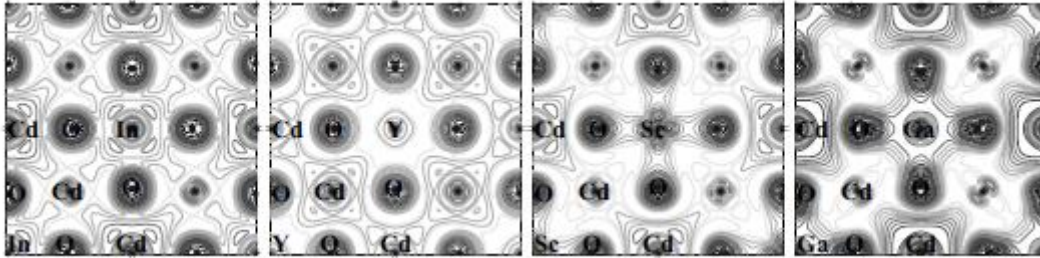
Fig.4: Contour plots of the charge density distribution in In, Y, Sc and Ga-doped CdO illustrate considerable electron localization around Sc and Ga ions as compared with In and Y cases where the charge density is more uniform. The plots are calculated in the xy plane within the 2kT energy window near the Fermi level. The grey scale increases with charge; the same scale is used for all plots. Atoms within one unit cell are labeled.

(iii) In and Y dopants preserve the uniform charge density distribution while Sc and Ga lead to significant electron localization around the dopant (Figure 4). The difference originates from the mismatch of the electronic configuration of the dopants and the energy location of the dopant empty *p* or *d* states with respect to the Fermi level. The Sc 3*d* states and Ga 4*p* states are energetically compatible with the conduction 5*s* states of Cd, while theY4*d* and In 5*p* are located higher in energy. As a result, the contributions from the Sc d or Ga *p* orbitals become significant near the Fermi level: the Sc d orbital contribution is dominant (85% of the Sc total) and the Ga *p* and *s* orbitals give comparable contributions (60% and 40%, respectively). The anisotropic Sc d or Ga *p* orbitals form strong directional bonds with the orbitals of the nearest oxygen atoms resulting in significant charge localization which is clearly seen from the charge density distribution plots (Figure 4).

(iv) The electron localization in Sc and Ga doped CdO results in a narrower conduction band and, hence, a reduction of the electron velocity as compared with In or Y (Table 2). Moreover, due to the high anisotropy of the Sc d or Ga p orbitals, a significantly reduced velocity is found in the Δ (Sc d orbitals) or Λ (Ga p orbitals) directions so that anisotropic transport properties are expected.

(v) The electron binding in Sc and Ga-doped CdO also leads to larger (in energy) optical transitions from the Fermi level (Ec in Figure 1), in contrast to the In and Y cases where the charge delocalization deminishes the second (hybridization) gap.

(vi) Finally, we note that even in the In, Yand F cases where the dopant ionic radius and electronic configuration are similar to that of Cd or O, the optical properties are worse than expected from the rigid band shift (CdO + e-) (Table 2). However, the calculated electron velocity and the density of states for In, Y and F-doped CdO are similar to those obtained from the rigid-band model (Table 2). Both factors contribute to the conductivity s, given by the expression:

$$\sigma = \frac{2e^2}{\Omega} \sum_{\mathbf{k}\lambda} |v_{\mathbf{k}\lambda}|^2 \tau_{\mathbf{k}\lambda} \delta(E_{\mathbf{k}\lambda} - E_F), \qquad (1.2)$$

so that the relaxation time τ will play the dominat role in determining the final carrier transport. [In Equation (1.2) e is the electron charge, Ω is the volume of the Brillouin zone, k is the wave vector, λ is the band index, v is the electron group velocity and E$_F$ is the Fermi energy.] Assuming that t is similar for all X3+ -doped systems, estimates of the Fermi electron velocity and the density of states at the Fermi level result in the trend In>Y>Sc>Ga, which is in agreement with experimental observations of the conductivity.

4.1 OXYGEN REDUCTION

Removal of an oxygen atom from a metal oxide leaves two extra electrons in the crystal. Whether one or both of these electrons become free carriers or remain localized at the vacancy site correlates with the oxide free energy of formation. In light metal oxides, such as CaO or Al_2O_3, where the formation energy is high, oxygen vacancies create deep charge localized states within the electronic band gap known as color or F centers. A relatively low formation energy of the conventional TCOs favors large oxygen deficiencies even under equilibrium growth conditions, giving rise to the free-carrier densities of 10^{17}–$10^{19}\,cm^{-3}$ for In_2O_3 and ZnO.

Electronic band structure investigations of oxygen deficient oxides showed that the oxygen defect $V_o^{\bullet\bullet}$ (in $Kr\ddot{o}ger-Vink$ notation the superscript $\bullet$ stands for effective positive charge) corresponds to a non-conducting state associated with the filling of the lowest single conduction band by the two vacancy-induced electrons. Only if the vacancy is excited, e.g. via a photoexcitation , or partially compensated to $V_o^{\bullet}$,does the single conduction band become half-occupied and conducting behavior may occur.

In oxygen deficient TCOs, the conduction band wave function resembles the one in the corresponding hosts, i.e. it is derived from the M s and O p states (Figure 1). A relatively uniform charge density distribution suggests that the vacancy-induced electrons are delocalized. However, a more thorough analysis of reduced In2O3 reveals that the metal atoms nearest to the oxygen defect give about two times larger contributions than the rest of the In atoms in the cell. As a result, there is a notable build-up of the charge density near the vacancy site. Importantly, the In atoms nearest the vacancy exhibit a reduction of the s-orbital contribution: the relative orbital contributions from the In s, p and d states are 81%, 8% and 11%, respectivly, in contrast to 97% s-orbital contributions from other In atoms in the cell. The high anisotropy of the p and d orbitals favors stronger covalent

(directional) bonds between the In atoms which surround the defect and their oxygen neighbors. These In–O pairs trap about 31% of the total charge density at the bottom of the conduction band. Similar behavior is found for other TCOs: in oxygen deficient CdO and ZnO, 18% and 39%, respectively, of the total charge density belong to the nearest (cation) and next nearest (oxygen) neighbors of the oxygen vacancy.

The presence of oxygen vacancies leads to significant changes in the electronic band structure of a TCO host. To illustrate the typical behavior, we compare the results obtained for oxygen deficient and Sn-doped In_2O_3 (Table 3 and Figure 5):

	Optical transitions (eV)		Fundamental band gap (eV)	Plasma frequency (eV)	Electron velocity $(\times 10^5 \, m\,s^{-1})$			$N(E_F)$
	E_v	E_c			$v^{[001]}$	$v^{[111]}$	$v^{[1\bar{1}1]}$	
$In_2O_3 + e^-$	3.01	0.54	1.16	2.35	9.42	9.45	8.60	1.51
$In_2O_3 + Sn^{\bullet}_{In}$	2.72	0.71	0.98	2.25	8.93	9.17	8.66	1.73
$In_2O_3 + V^{\bullet}_O$	2.07	1.11	0.71	1.32	5.58	6.42	4.81	3.36

Table3: Properties of oxygen-deficient and Sn-doped In2O3 as obtained from electronic band structure calculations within local density approximation. Values for undoped stoichiometric In2O3 found from a rigid band shift are given for comparison. The electron concentration is $1.95 \times 10^{21} \, cm^{-3}$ for all systems. The plasma frequency is calculated from Equation (1.3)

(i) Strong structural relaxation around the vacancy reduces the distance between the In and O atoms nearest to the defect to 2.12Å(on average). This leads to an increased In–O distances for the atoms located further from the defect and, hence, to a weaker Ins–Op hybridization. As a result, the fundamental band gap and the optical transitions from the valence band (Ev) are significantly reduced in oxygen-deficient In2O3 as compared with Sn-doped oxide.

(ii) Owing to the stronger binding between the In and O atoms nearest to the defect, the lowest single conduction state occupied by the vacancy-induced electrons is split from the rest of the conduction band by a second gap. In marked contrast, the second gap is absent in the substitutionally doped oxide. This is a manifestation of a more uniform spatial charge density distribution, i.e. the charge delocalization. Note, the second gap previously reported for Sn-doped In_2O_3 vanishes upon structural relaxation around Sn ions [Figure 5(b)].

(iii) The increased charge density in the vicinity of the oxygen vacancy and the related narrowing of the conduction band give rise to the reduced electron velocity (Table 3). At the same time, the density of states near the Fermi level increases. Since both factors contribute to the conductivity [Equation (1.2)], the difference in the charge transport of the oxygen-deficient and Sn-doped In2O3 will be determined primarily by the relaxation time   in the same equation. Qualitatively, the stronger structural relaxation with the atomic displacements around the oxygen vacancy being twice as large as those around Sn ions, implies a stronger charge scattering in oxygendeficient oxide. In addition, a shorter electron relaxation time in this case should be expected due to the Coulomb attraction of the free carriers to   associated with its higher formation energy compared with that of   , which is the ground-state defect . Moreover, due to the strong preference of the extra electrons to bind with   to form   , the charge transport will be adversely affected since the latter defect corresponds to a nonconducting state (a completely filled single conduction band).

(iv) Due to the narrower conduction band in the oxygen-deficient oxide, the plasma frequency is expected to be significantly smaller than

that in Sn-doped material. The plasma oscillations affect the optical properties: the electromagnetic waves offrequency below (and wavelength above) ω_p are reflected due to the electronscreening. The plasma frequency is given by the expression:

$$\omega_p^2 = \frac{8\pi e^2}{3\Omega} \sum_{\mathbf{k}\lambda} |v_{\mathbf{k}\lambda}|^2 \delta(E_{\mathbf{k}\lambda} - E_F), \qquad (1.3)$$

where e is the electron charge, Ω is the volume of the Brillouin zone, **k** is thewave vector, λ is the band index, v is the electron group velocity and E_F is the Fermi energy. Our estimates for ω_p in the oxygen-reduced and Sn-doped In_2O_3 as well as the one obtained from the rigid band model are given in Table 3.

In summary, compared with substitutional doping, oxygen reduction of a TCO host may result in higher carrier densities but would limit the electron mobility due to shorter relaxation times and considerable charge trapping near the vacancy site. Also, a weaker Ms–Op hybridization due to stronger structural relaxation around the vacancy significantly reduces the optical transparency window.

There may be other native point defects that give rise to a conducting behavior in a TCO. For example, it was shown that interstitial Sn ions in SnO_2 have low formation energies and produce donor levels inside the conduction band of this material. In this case, significant structural rearrangement associated with the formation of Sn(II)O bonds as in SnO is expected to have an even stronger effect on the properties of the oxide host and to increase electron scattering.

The above considerations demonstrate the advantages of employing substitutional doping as a primary carrier generation mechanism in conventional TCO hosts. However, notwithstanding the above limitations, we believe that varying the degree of nonstoichiometry may serve as a versatile tool for optimizing a TCO's overall performance.

5. TRANSPARENT ELECTRONICS DEVICES

In order to produce a transparent-electronics-based system, appropriate materials must be selected, synthesized, processed, and integrated together in order to fabricate a variety of different types of devices. In turn, these devices must be chosen, designed, fabricated, and interconnected in order to construct circuits, each of which has to be designed, simulated, and built in such a way that they appropriately function when combined together with other circuit and ancillary non-circuit subsystems. Thus, this product flow path involves materials → devices → circuits → systems, with each level of the flow more than likely involving multi-feedback iterations of selection, design, simulation, fabrication, integration, characterization, and optimization.

From this perspective, devices constitute a second level of the product flow path. The multiplicity, performance, cost, manufacturability, and reliability of available device types will dictate the commercial product space in which transparent electronics technology will be able to compete. Thus, an assessment of the device toolset available to transparent electronics is of fundamental interest, and is the central theme of this chapter.

Passive, linear devices - resistors, capacitors, and inductors – comprise the first topic discussed. Passive devices are usually not perceived to be as glamorous as active devices, but they can be enabling from a circuit system perspective, and they are also the simplest device types from an operational point-of-view. Together, these two factors provide the rationale for considering this topic initially.

Next, two-terminal electronic devices - pn junctions, Schottky barriers, heterojunctions, and metal-insulator-semiconductor (MIS) capacitors - constitute the second major topic. The motivation for this topical ordering is again associated with their relative operational complexity, rather than their utility. The

third and final major topic addressed is transistors. This is the most important matter considered in this chapter. Most of this discussion focuses on TTFTs, since they are perceived to be the most useful type of transistor for transparent electronics. Additionally, a very brief overview of alternative transistor types - static-induction transistors, vertical TFTs, hot electron transistors, and nanowire transistors - is included. This is motivated by recognizing the desirability of achieving higher operating frequencies than are likely obtainable using TTFTs with minimum gate lengths greater than ~2-10 μm, a probable lower-limit dimensional constraint for many types of low-cost, large-area applications. Alternative transistors such as these offer possible routes for reaching higher operating frequencies, in the context of transparent electronics.

6. PASSIVE, LINEAR DEVICES

A passive device absorbs energy, in contrast to an active device, which is capable of controlling the flow of energy (Spencer and Ghausi 2003). A linear device is distinguished by the fact that its input-output characteristics are describable using a linear mathematical relationship. The three passive, linear devices of interest are resistors, capacitors, and inductors.

6.1 RESISTORS

An ideal resistor is a device whose current-voltage characteristics are linear, described by Ohm's Law, and which dissipates power if a voltage exists across it. The two foundational ideal resistor device equations are indicated by the first two entries in Table 4.

A real resistor may not be perfectly linear, i.e., precisely obey Ohm's Law, and may also possess some undesirable capacitive or inductive parasitic characteristics. Transparent thin-film resistors (TTFRs) are expected to operate at relatively low frequencies, so that parasitic inductance is not anticipated to be relevant. Additionally, TTFRs will most likely be fabricated on insulating substrates, so that parasitic capacitance should be minimal. Finally, if properly designed, a TTFR is expected to exhibit linear or very near-linear behavior. Thus, in most respects, we expect a TTFR to be adequately modeled as an ideal resistor.

An equation for the resistance of a TTFR is given by the third entry in Table 4. The resistance depends on a material property, namely the resistivity of the TTFR layer, and the geometry, which is assumed to be rectangular for the situation considered in Table 4. Given this geometrical constraint, if the current path length is assumed to be equal to the crosssectional width, i.e., if L = W, and

if a sheet resistance is defined as RS = ρ/t, then the resistance depends simply on RS and the number of resistor squares in the TTFR layout.

Quantity Assessed	Equation
Voltage (instantaneous)	$v(t) = i(t)R$ (Ohm's Law)
Power dissipated (instantaneous)	$p(t) = i(t)v(t)$
TTFR resistance	$R = \dfrac{\rho L}{A} = \dfrac{\rho L}{Wt} = \dfrac{\rho}{t}\dfrac{L}{W} = R_S n$

t = time (s)
i(t) = current (instantaneous) (A)
R = resistance (Ω)
ρ = resistivity (Ω-cm)
L = current path length (cm)
A = current path cross-sectional area (A = Wt) (cm^2)
W = current path cross-sectional width (cm)
t = thin-film thickness (cm)
R_S = sheet resistance ($\Omega\ \square^{-1}$)
n = number of squares, i.e. $n = \left.\dfrac{L}{W}\right|_{L=W}$ (unitless)

Table 4: A summary of resistor device equations.

Figure 5 a shows a plan-view of a straight-line or linear TTFR. The TTFR path consists of 16 squares, with two larger end squares, generically illustrating one possible resistor termination scheme. Many variations on resistor termination are possible. A more complicated, meandering TTFR layout with 36 path squares is given in Figure 5b. This TTFR occupies approximately the same area as the straight-line TTFR of Fig. 5 a, but possesses a larger resistance because of the larger number of squares in its path and also due to the existence of bends in

the meander structure, which increase the resistance (Glaser and Subak-Sharpe 1979; Elshabini-Riad and Barlow 1998).
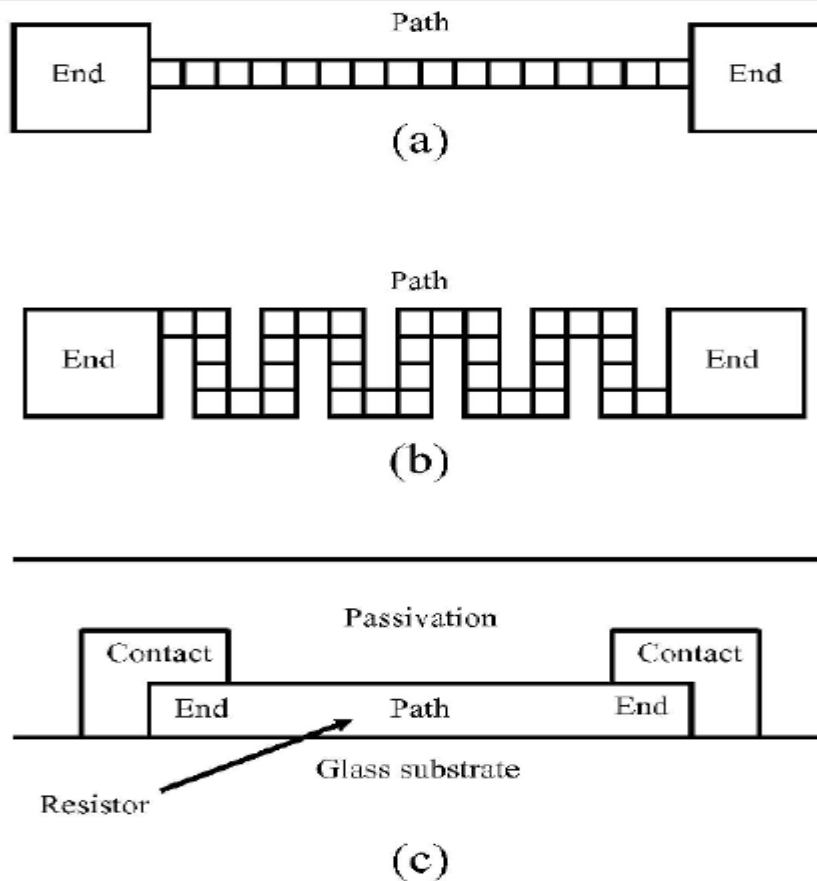

Fig 5: (a) Plan-view of a straight-line or linear transparent thin-film resistor (TTFR) and (b) a meander TTFR. (c) Cross-sectional view of a TTFR in which contacts and passivation are also indicated.

Figure 5 c offers a cross-sectional view of a TTFR in which the resistor path and ends have the same thickness, which need not always be the case. Contacts from the resistor ends to other locations on the substrate are indicated, as is a passivation layer. If the TTFR layer is heavily doped, e.g., ITO, the passivation layer's role is merely to provide physical and chemical protection. However, it is possible that a passivation layer may actually play an active role in establishing

the TTFR resistance if a highly insulating layer is used in the resistor path and its conductance is established by creation of a surface accumulation layer due to the presence of the passivation layer. In this case, the resistance would not scale with the TTFR thickness, but would be controlled by the surface accumulation charge due to interface properties and charge within the passivation layer.

TTFR sheet resistances of ~10-105 Ω/□ should be possible, using doped TCOs such as ITO or undoped TTFT channel layers such as ZTO. Thus, a wide range of TTFR resistance is possible.

Two thin-film resistor concerns are the desire to have a small temperature coefficient of resistance (TCR) and resistor tolerance. Near-zero temperature coefficient of resistance values have been demonstrated for antimony- doped SnO_2, with an appropriate doping concentration (Maissel and Glang 1970). TTFR resistance tolerance is expected to be similar to that of conventional thin-film resistors, ±10%, unless resistor trimming is performed, in which case a tolerance of approximately ±0.1% is possible (Glaser and Subak-Sharpe 1979; Elshabini-Riad and Barlow 1998). It is not clear whether resistor trimming will be practical in a transparent electronics technology, given its anticipated low-cost structure. Smooth surfaces are highly desirable for TTFR applications, suggesting that amorphous layers would be preferred.

6.2 CAPACITORS

An ideal capacitor is an electric field energy storage device possessing linear current-voltage derivative (i-dv/dt) characteristics. Defining ideal capacitor equations are collected in the first three entries of Table 5.

A plan-view and a cross-sectional view of a transparent thin-film capacitor (TTFC) are given in Fig. 6. In order for this device to be completely transparent, all of the layers should be transparent. Most insulators are transparent, so that

this constraint mainly applies to the contact layers, which will most likely be highly conducting TCOs such as ITO. Alternative TTFC structures, e.g., interdigitated capacitors (Glaser and Subak-Sharpe 1979; Elshabini-Riad and Barlow 1998), are possible in addition to the simple TTFC structure shown in Fig.6.

Quantity Assessed	Equation
Charge (instantaneous)	$q(t) = Cv(t)$
Current (instantaneous)	$i(t) = C\dfrac{dv(t)}{dt}$
Energy stored (instantaneous)	$w(t) = \dfrac{1}{2}C[v(t)]^2$
TTFC capacitance	$C = \dfrac{\varepsilon_I A}{d_I} = \dfrac{\varepsilon_I LW}{d_I}$

t = time (s)
C = capacitance (F)
v(t) = voltage (instantaneous) (V)
ε_I = insulator dielectric constant (F cm^{-1})
A = capacitor area (A = LW; see Fig. 5.2) (cm^2)
d_I = dielectric thickness (cm)

Table 5:A summary of capacitor device equations.

The primary TTFC design equation is included as the fourth entry in Table 5. The TTFC capacitance is established by the capacitance density, i.e., the capacitance per unit area, of the basic capacitance stack, i.e., εS/dI, and the geometric area of the capacitor layout. Usually a large capacitance density is desired, in order to minimize the size of a capacitor. Therefore, a thin insulator with a high dielectric constant (sometimes referred to as a 'high-k dielectric',

where 'k' denotes the relative dielectric constant) is best. However, a high-k dielectric typically has a smaller bandgap, which usually results in a low breakdown electric field. Although reducing the insulator thickness also increases the capacitance density, a minimum thickness is required to avoid pinholes and other types of defects which degrade the breakdown field and which yield more insulator leakage. Optimal TTFC and TTFT gate insulators will
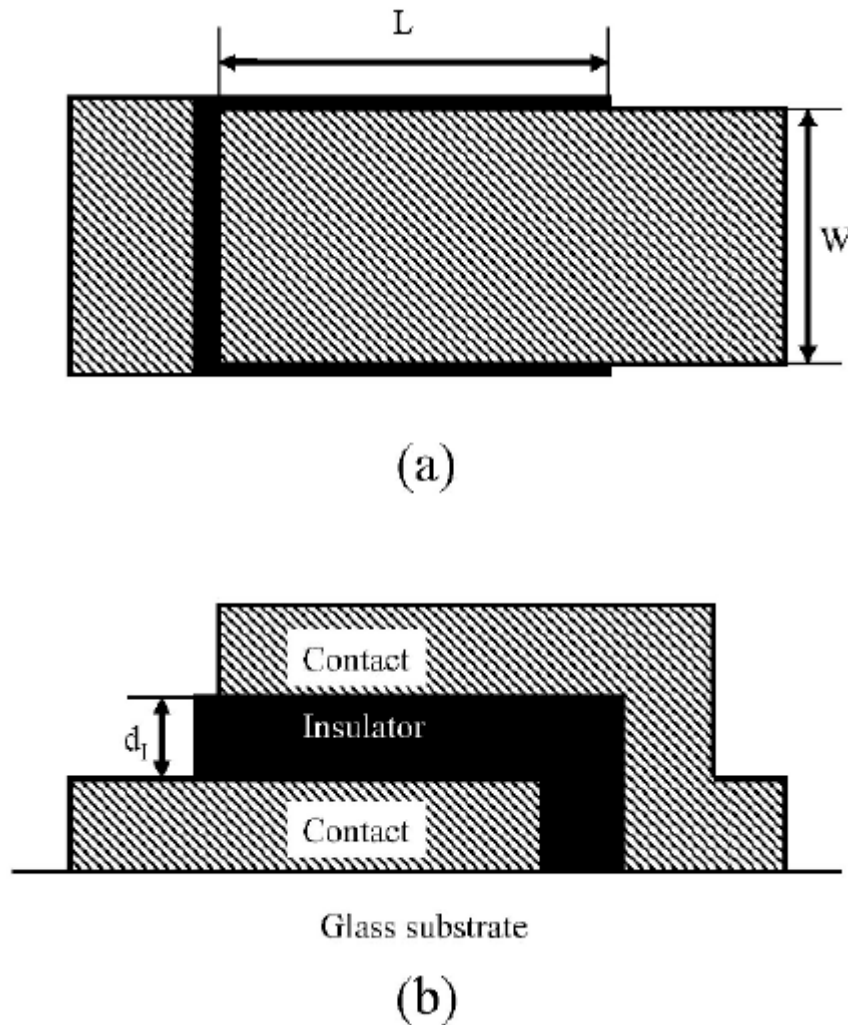

Fig.6: (a) Plan-view and (b) cross-sectional view of a transparent thin-film capacitor (TTFC).

have maximal dielectric constant-breakdown field products (Ono 1995). For a more detailed discussion of insulators and thin-film capacitors the interested reader is referred to the following references (Maissel and Glang 1970; Glaser and Subak-Sharpe 1979; Elshabini-Riad and Barlow 1998; Ono 1995; Kao 2004).

Real TTFCs are expected, for most purposes, to be accurately modeled as ideal capacitors. Although TTFC performance may be degraded by inductive and resistive parasitic effects, neither of these are expected to be severe given that these devices are expected to be used at relatively low frequencies and that low-leakage thin-film insulators are already employed in non-transparent applications. From process integration, manufacturability, and reliability considerations, TTFC contacts and insulators should ideally be amorphous.

6.3 INDUCTORS

An ideal inductor is a magnetic field energy storage device possessing linear voltage-current derivative (v-di/dt) characteristics. Important ideal inductor equations are collected in the first two entries of Table 6.

In contrast to a TTFR and a TTFC, a transparent thin-film inductor (TTFI) and related transparent magnetically-coupled devices are expected to behave in a non-ideal manner. Two main reasons underlie this expectation. First, because of the relatively poor conductance of TCOs compared to metals, TTFIs will possess a significant amount of parasitic resistance. Second, efficient magnetic field coupling is strongly facilitated by the use of a magnetically-permeable insulator. However, we are not aware of a transparent, magnetically-permeable insulator material. Thus, realizing high performance TTFIs and related magnetically-coupled devices is expected to be a challenging task.

The last two entries included in Table 6 are useful for understanding certain aspects of TTFI non-idealities. The quality factor, Q, is basically an inductor

performance figure-of-merit. A larger Q is better. Thus, since the parasitic resistance of a TTFI is expected to be large, as a consequence of employing a TCO instead of a metal, high-Q TTFI's are not expected. The last entry in Table 6 indicates that obtaining a large inductance, L, requires the inductor to cover a large area and to possess a large number of turns. The large-area requirement is not necessarily problematic, since 'real estate' if often 'free' in transparent electronics. However, needing to have a large number of turns is likely to cause trouble, since having a large number of turns will increase the inductor parasitic series resistance, and probably also the inductor parasitic capacitance.

Quantity Assessed	Equation
Voltage (instantaneous)	$v(t) = L\dfrac{di(t)}{dt}$
Energy stored (instantaneous)	$w(t) = \dfrac{1}{2}L[i(t)]^2$
Quality factor	$Q = \dfrac{2\pi f L}{R_L}$
Inductance (rectangular spiral inductor)	$L \propto SN^2$ (Kovacs 1998)
t = time (s) L = inductance (H) i(t) = current (instantaneous) (A) f = frequency (Hz) R_L = inductor parasitic resistance (Ω) S = maximum side dimension (cm) N = number of turns (unitless)	

Table 6: A summary of inductor device equations.

These TTFI challenges are disappointing since a TTFI and its magnetically-coupled device variants are potentially application-enabling, performance-enhancing components. Inductors are useful in resonant circuits and filters. They can also function as power supply chokes (limiting current fluctuations), energy storage devices for switched-mode power supplies, etc. Furthermore, magnetically-coupled inductors may be used for the construction of transformers for power and signal conditioning. Finally, a somewhat-related application is that of an antenna to transmit or receive rf signals. In this regard, we note that a transparent microwave antenna constructed using ITO has been reported (Outaleb et al. 2000).

Even though a TTFI with good performance appears to be difficult to construct, the benefits of magnetic field coupling devices appear to offer enough enticements to warrant further investigation.

7. TRANSPARENT THIN-FILM TRANSISTORS (TTFTs)

TTFTs constitute the heart of transparent electronics. The first two sections focus on ideal and non-ideal behavior of n-channel TTFTs. Next, n-channel TTFT stability is considered. Finally, issues related to alternative device structures – double-gate TTFTs and the realization of p-channel TTFTs - are discussed.
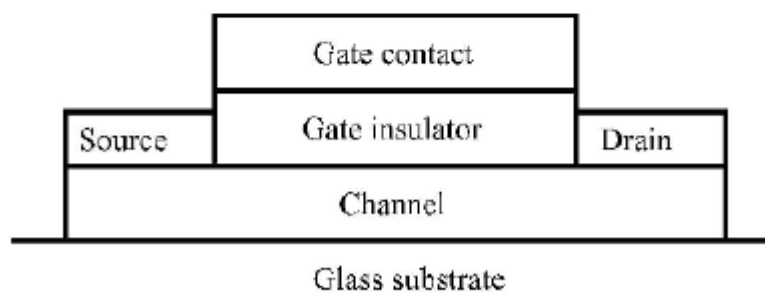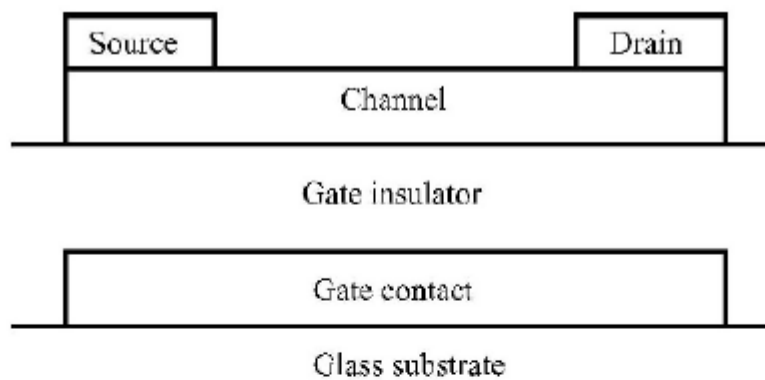

(a)

(b)

Fig.7: Two possible transparent thin-film transistor (TTFT) device structures,(a) a staggered, bottom-gate, and (b) a coplanar, top-gate.

Figure 7. illustrates two of four possible TTFT device structures. The first one, considered in Fig. 7a, is denoted as a staggered, bottom-gate since source-drain and gate contacts are located at the top and bottom of the device, respectively. Figure 7b shows a coplanar, top-gate structure in which the source-drain and the gate are all positioned on the top side of the TTFT. The remaining two TTFT device structures, not shown, are the staggered, top-gate and coplanar, bottom-gate configurations. Although in a conventional TFT, the source, drain, and gate contact materials would be metals, a highly conductive TCO, such as ITO, is used in a TTFT. Additionally, while the channel layer of a conventional TFT employs a narrow band gap, opaque semiconductor, a highly insulating, wide band gap transparent semiconductor is used in a TTFT.

Ideal operation of an n-channel TTFT is described as follows.

With the source grounded, a positive voltage is applied to the drain in order to attract electrons from the source to the drain. The amount of drain current, ID, which flows from the source to the drain depends upon whether or not an electron accumulation layer exists at the channel-insulator interface. No drain current flows if the gate-source voltage, V_{GS}, is less than the turn-on voltage, V_{ON}, since electrons are not present in the channel. This situation is indicated in Fig. 8a. Thus, it is the low carrier concentration nature of the channel which holds off the flow of drain current between the source and the drain for V_{GS}'s below V_{ON}.

If a gate voltage, V_{GS}, greater than V_{ON} is applied while a positive voltage exists at the drain, i.e., if V_{DS} is positive, drain current flows, as indicated in Fig. 8b. Physically, electrons are injected from the source into the gate-bias-induced electron accumulation layer channel, are transported across this low-resistance

accumulation layer, and are extracted at the drain contact. This electron transport process corresponds to the flow of drain current in the opposite direction, from the drain to the source. The magnitude of drain current flowing depends on the gate overvoltage, i.e., on V_{GS}-V_{ON}, which determines the accumulation layer sheet charge density, and also on the magnitude of the drain voltage, which establishes the electric-field aided drift condition along the channel, from the source to the drain. For small VDS's compared to the gate overvoltage (i.e., for V_{DS}<<V_{GS}-V_{ON}), drain current flow in the channel is describable using Ohm's law, i.e., I_D = V_{DS}/R_C(V_{GS}), where R_C(V_{GS}) is the resistance of the channel, indicating that electron transport across the channel may be modeled as simply resistive. In fact, the channel resistance is indicated in Ohm's law in the functional form R_C(V_{GS}) since the channel resistance depends on the accumulation layer sheet charge density, which is controlled by V_{GS}.

As the magnitude of this applied positive drain voltage increases so that V_{DS} is no longer negligible compared to the overvoltage (V_{GS}-V_{ON}), I_D is no longer Ohmic with respect to VDS, but, rather, becomes sublinear and eventually saturates when channel pinch-off occurs at V_{DS}≡V_{DSAT}=V_{GS} - V_{ON}.

Pinch-off may be understood quantitatively by recognizing that the electron accumulation layer sheet charge density is given by $Q_n(y)$=C_G[V(y)- V_{ON}], where V(y) is the channel-insulator interfacial voltage drop along the channel from the source to the drain, with y=0 and y=L corresponding to distances along the channel at the edge of the source and the edge of the drain, respectively. At the drain edge of the channel, $Q_n(L)$=C_G[V_{GS}-V_{DS}-V_{ON}]. Thus, the accumulation layer sheet charge density is equal to zero at y=L, and the channel is therefore depleted or 'pinched off', when the term in the square brackets goes to zero, leading to the pinch-off relationship as specified by the first entry in Table 7. This nonlinear, pre-pinch-off to saturated, post-pinch-off situation is sketched in Fig. 8c, attempts to capture both the drain voltage-induced elimination of the electron

accumulation layer channel near the drain-end of the channel, and the inherently 2- dimensional nature of the TTFT electric field near the drain in this regime of device operation.
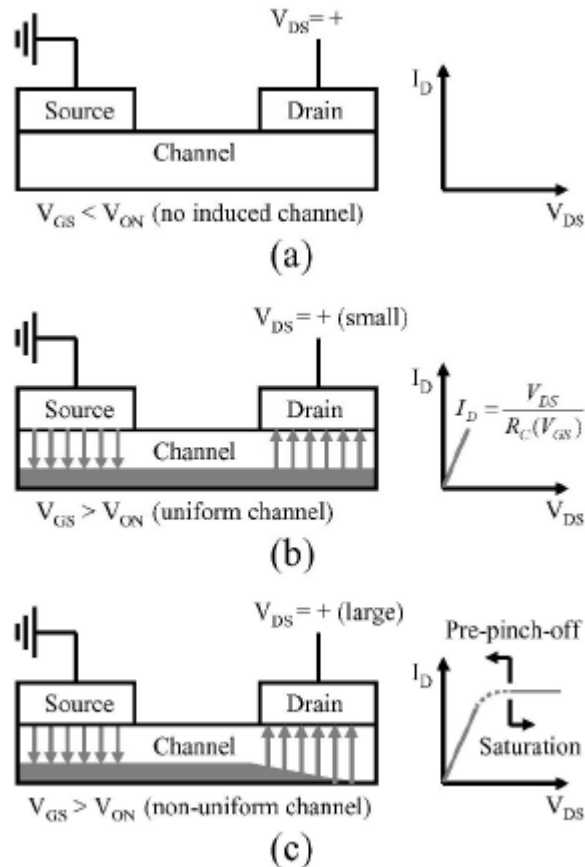
Fig.8: Ideal n-channel transparent thin-film transistor (TTFT) operation. (a) Cut-off. Zero drain current ($I_D=0$) occurs in cut-off, which is defined by $V_{GS}<V_{ON}$, and corresponds to a situation in which no electron accumulation layer exists at the channel-gate insulator interface. (b) Linear, pre-pinch-off. I_D is described by Ohm's law [$I_D=V_{DS}/R_C(V_{GS})$] at low V_{DS}'s [$V_{DS}<<V_{GS}-V_{ON}$], corresponding to the formation of a uniform electron accumulation layer at the channelgate insulator interface from the source to the drain. (c) Nonlinear, pre-pinch-off and, post-pinch-off, saturation. ID becomes sublinear with respect to VDS and then saturates when $V_{DS}\equiv V_{DSAT}=V_{GS}-V_{ON}$ because of the depletion or 'pinch-off' of the

electron accumulation layer at the channel-gate insulator interface near the drain. V_{DSAT} defines the boundary between pre-pinch-off and post-pinch-off or saturation.

Quantity Assessed	Equation
Pinch-off condition (V)	$V_{DSAT} = V_{GS} - V_{ON}$
Drain current (A)	$I_D = 0$ (cut-off; $V_{GS} < V_{ON}$) $I_D = \dfrac{W}{L} \mu C_G \left[(V_{GS} - V_{ON}) V_{DS} - \dfrac{V_{DS}^2}{2} \right]$ (pre-pinch-off; $V_{GS} \geq V_{ON}$, $V_{DS} \leq V_{DSAT}$) $I_D \equiv I_{DSAT} = \dfrac{W}{2L} \mu C_G (V_{GS} - V_{ON})^2$ (post-pinch-off or saturation; $V_{GS} \geq V_{ON}$, $V_{DS} > V_{DSAT}$)
V_{DSAT} = drain-source voltage defining the onset of saturation (V) V_{GS} = gate-source voltage (V) V_{ON} = turn-on voltage (V) W = gate width (μm) L = gate length (μm) μ = channel mobility (cm^2 V^{-1}s^{-1}) C_G = gate capacitance density (F cm^{-2}) V_{DS} = drain-source voltage (V) I_{DSAT} = saturation current (A)	

Table 7: A summary of ideal, square-law theory TTFT device equations.

A quantitative formulation of ideal TTFT operation is given according to square-law theory (Borkan and Weimer 1963; Tickle 1969; Hong et al. 2007), as summarized in Table 7. Note that the linear or Ohmic regime, as indicated in Fig. 8b, corresponds to the pre-pinch-off limit in which $V_{DS} << V_{GS} - V_{ON}$ so that $I_D \approx (W/L) \mu C_G (V_{GS} - V_{ON}) V_{DS}$, which means that $R_C(V_{GS}) = (W/L) \mu C_G (V_{GS} - V_{ON})$. Ideal aspects of square-law theory include the absence of subthreshold current (i.e., the subthreshold swing, S=0) and hard saturation of the drain current characteristics (i.e., in saturation, $dI_D/dV_{DS} = 0$).

8. APPLICATIONS

As the oxide semiconductors are wide band gap materials, transparent TFTs can be easily realized by the combination of transparent electrodes and insulators. Transparency is one of the most significant features of TAOS TFTs. As the band gap of a-Si is 1.7 eV and that of crystalline-Si is 1.1 eV, 'transparent electronics' cannot be realized in Si technology. In TAOS TFTs, features of high mobility or low process temperature have attracted a lot of attention. However, transparency has been underestimated or even neglected in the research and development of TAOSs. Few examples of actual applications have been reported exploiting the transparency of TAOSs until now [25, 26]. Transparent circuits will have unprecedented applications in flat panel displays and other electronic devices, such as seethrough display or novel display structures. Here, practical examples taking advantage of the transparency of TAOS TFTs are: Reversible Display, 'Front Drive' Structure for Color Electronic Paper, Color Microencapsulated Electrophoretic Display, Novel Display Structure – Front Drive Structure. Indium oxide nanowire mesh as well as indium oxide thin films were used to detect different chemicals, includingCWA simulants.

9. FUTURE SCOPE

It should be apparent from the discussion that although much progress has been made in developing new materials and devices for high performance transparent solar cells, there is still plenty of opportunity to study and improve device performance and fabrication techniques compared with the nontransparent solar cell devices. In particular, the stability of transparency solar cells has not been studied yet. Solution-processable transparent PSCs have become a promising emerging technology for tandem solar cell application to increase energy conversion efficiency. The transparency of solar cells at a specific light band will also lead to newapplications such as solar windows. The field of energy harvesting is gaining momentum by the increases in gasoline price and environment pollution caused by traditional techniques. Continued breakthroughs in materials and device performance, accelerate and establish industrial applications. It is likely that new scientific discoveries and technological advances will continue to crossfertilize each other for the foreseeable future.

10.CONCLUSION AND REMARKS

Oxides represent a relatively newclass of semiconductor materials applied to active devices, such as TFTs. The combination of high field effect mobility and lowprocessing temperature for oxide semiconductors makes them attractive for high performance electronics on flexible plastic substrates. The marriage of two rapidly evolving areas of research, OLEDs and transparent electronics, enables the realization of novel transparent OLED displays. This appealing class of see-through devices will have great impact on the human–machine interaction in the near future. EC device technology for the built environment may emerge as one of the keys to combating the effects of global warming, and this novel technology may also serve as an example of the business opportunities arising from the challenges caused by climate changes The transparency of solar cells at a specific light band will also lead to newapplications such as solar windows. The field of energy harvesting is gaining momentum by the increases in gasoline price and environment pollution caused by traditional techniques.

11.REFERENCE

'Transparent Electronics ', Springer publications, J.F.Wager, D. A. Keszler, R. E. Presley.

'Transparent electronics: from synthesis to applications', Wiley publications: Antonio Facchetti, Tobin J. Marks.

www.wikipedia.org

www.ieee.org

www.sciencemag.org

www.wiley.com